Influences of Hall Effect on the Magnetohydrodynamic Behavior of Two Axially Colliding Field-Reversed Configurations*)

Kei MATSUZAKI, Shintaro KOIKE, Masahiro YANAGI, Naoki MIZUGUCHI[1)] and Toshiki TAKAHASHI

Division of Electronics and Informatics, Gunma University, Kiryu, Gunma 376-8515, Japan
[1)]*National Institute for Fusion Science, Toki, Gifu 509-5292, Japan*

(Received 30 November 2015 / Accepted 26 April 2016)

We report here the simulation results of two colliding accelerated field-reversed configurations (FRCs). In our simulation code, we separately modeled the external magnetic field and that generated by plasma. By using a time-variable external magnetic field, we reproduced the translation of FRCs. Since the Hall effect is expected to play an important role in the magnetic reconnection research, we employed both the 2D resistive magnetohydrodynamic (MHD) model and the 2D resistive Hall-MHD model. We compare the simulation results and report on the changes in the properties of plasma.

Keywords: field-reversed configuration, translation, merging, magnetic reconnection, simulation, Hall MHD

DOI: 10.1585/pfr.11.2403097

1. Introduction

Field-reversed configurations (FRCs) are in an ultrahigh beta state [1], and consequently, they are attractive as core plasmas in advanced fuel fusion reactors. A conventional FRC plasma formed following the theta-pinch method, however, maintains the field reversal for less than or a few 100 μs. Recently, a long-lived FRC was observed in a C-2 experiment (i.e., axial collision of two accelerated FRCs and subsequent merging) conducted by Tri Alpha Energy, which was sustained for more than a few milliseconds [2]. A simple estimation shows that approximately 60% of the translation energy is converted into thermal energy of confined plasma [3].

In order to study the collision and merging process of two accelerated FRCs, numerical simulations are beneficial so as to understand short-time phenomena and the time evolution of physical quantities. The FRC translation formed by a conical theta pinch is calculated by the MOQUI code [4]. In addition, the acceleration and translation of FRCs are computed by the NIMROD code [5], which is widely used for compact torus plasmas. In this sense, there are a few numerical works in the literature on collision and merging processes between two accelerated FRCs. Although the results obtained using the Lamy Ridge code are presented in Ref. [3], their calculation model was not available. The Lamy Ridge simulation results showed that the plasma temperature within the separatrix of merged FRCs is elevated due to a strong rethermalization.

Magnetic reconnection [6] is an essential process in the merger of two FRCs. This phenomenon can be observed in solar flares, and it can be seen in a compact torus plasma experiment. From numerous TS-3/4 spheromak merging experiments, the stability and confinement properties have been found to depend on the polarity of the toroidal field and/or the averaged Larmor radius [7]. Moreover, anomalous resistivity and current have been observed in the magnetic reconnection region, and the reconnection speed is significantly dependent on the chosen resistivity model [8, 9].

In the present work, we study the role of two-fluid effects by including the Hall term to the resistive magnetohydrodynamic (MHD) equations. In the two-dimensional (2D) resistive MHD model, both the toroidal flow velocity and magnetic field vanish when initially nonrotating FRC plasma is considered. In contrast to the 2D resistive model, the toroidal flow and magnetic field emerge in the frame of the Hall-MHD model. We therefore are interested in finding the mechanism of the toroidal field within a translation process and examining the two-fluid Hall effect in two FRCs collision process and subsequent merging process.

2. Simulation Model

Our simulation code uses the cylindrical coordinate system and solves the resistive MHD and Hall-MHD equations described below. The Hall term is the last term on the right-hand side of Eq. (4).

$$\frac{\partial \rho}{\partial t} = -\nabla \cdot (\rho \mathbf{u}), \tag{1}$$

$$\frac{\partial \mathbf{u}}{\partial t} = -(\mathbf{u} \cdot \nabla)\mathbf{u} - \frac{1}{\rho}\left(\nabla p - \mathbf{j} \times \mathbf{B} + \nabla \cdot \overleftrightarrow{\Pi}\right), \tag{2}$$

author's e-mail: t-tak@gunma-u.ac.jp

*) This article is based on the presentation at the 25th International Toki Conference (ITC25).

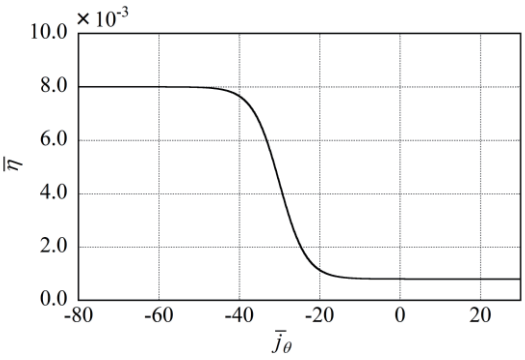

Fig. 1 Relationship between resistivity η and current density j_θ.

$$\frac{\partial p}{\partial t} = -(\mathbf{u}\cdot\nabla)\,p - \gamma\, p\nabla\cdot\mathbf{u} + (\gamma-1) \times\left\{\eta|\mathbf{j}|^2 - \overleftrightarrow{\Pi} : \nabla\mathbf{u}\right\}, \tag{3}$$

$$\frac{\partial \mathbf{B}}{\partial t} = \nabla\times(\mathbf{u}\times\mathbf{B}) - \nabla\times(\eta\,\mathbf{j}) - \nabla \times\left[\frac{1}{en_\mathrm{e}}[(\mathbf{j}\times\mathbf{B}) - \nabla p_\mathrm{e}]\right], \tag{4}$$

$$\mu_0\mathbf{j} = \nabla\times\mathbf{B}, \tag{5}$$

$$\overleftrightarrow{\Pi} = -\mu\left[\nabla\mathbf{u} + (\nabla\,\mathbf{u})^\mathrm{T} - \frac{2}{3}\overleftrightarrow{I}\,(\nabla\cdot\mathbf{u})\right], \tag{6}$$

$$p_\mathrm{e} = \alpha p, \quad n_\mathrm{e} = n_\mathrm{i} = \rho/m_\mathrm{i}. \tag{7}$$

Here ρ, $\mathbf{u}$, and p are the mass density, flow velocity, and pressure of the deuterium plasma, respectively. Moreover, $\mathbf{B}$ and $\mathbf{j}$ are the magnetic field and current density, respectively. The electron pressure p_e and density n_e are determined by Eq. (7), where m_i is the deuterium mass. The specific heat ratio γ is 5/3, and e and μ_0 are the elementary charge and vacuum permeability, respectively. In this simulation, the viscosity coefficient μ is assumed to be constant. We consider the nonuniform resistivity model. Figure 1 shows the relationship between the resistivity η and the current density. In the present model, the resistivity is a function of the current density and is written in the following form:

$$\eta = \frac{\eta_\mathrm{min} - \eta_\mathrm{max}}{1 + \exp\left[-A(\bar{j}_\theta - \bar{j}_\mathrm{h})\right]} + \eta_\mathrm{max}. \tag{8}$$

This is known as the sigmoid function. In Eq. (8), η_min, η_max, A, and j_h are the parameters to control the shape of the curve in Fig. 1, where η and j_θ are normalized by $\mu_0 r_\mathrm{w} v_\mathrm{A0} = 9.6\times10^{-3}\,\Omega\cdot\mathrm{m}$ and $\psi_\mathrm{w}/(2\mu_0 r_\mathrm{w}^3) = 3.0\times10^5\mathrm{A/m}^2$, respectively. Here we set $A = 0.3$, $\bar{j}_\mathrm{h} = -30$, $\bar{\eta}_\mathrm{min} = 8.0\times10^{-4}$, and $\bar{\eta}_\mathrm{max} = 8.0\times10^{-3}$, which correspond to $\eta_\mathrm{max} = 7.7\times10^{-5}$ and $\eta_\mathrm{min} = 7.7\times10^{-6}\,\Omega\cdot\mathrm{m}$, respectively. The value of η_max is significantly large compared to the classical resistivity $\eta_\mathrm{cl} = 1.4\times10^{-6}\,\Omega\cdot\mathrm{m}$ for a 100 eV plasma. In this work, the plasma current in the FRC core is defined as positive along the toroidal direction. Conversely, the current sheet generated between two adjacent FRCs is in the opposite direction to the core current and has a negative sign. Therefore, our model accounts for a large resistivity within the current sheet region and aims at providing a fast reconnection process.

Table 1 Plasma and calculation parameters.

Parameter	Value [Unit]
Radius of the confinement region, r_w	0.17 [m]
External field, B_ex	0.4 [T]
Magnetic flux on the machine wall, ψ_w	3.76×10^{-3} [Wb]
Ion temperature, T_i	100 [eV]
Alfvén time, $r_\mathrm{w}/v_\mathrm{A0}$	3.63×10^{-6} [s]
Alfvén speed, v_A0	4.68×10^4[m/s]
Time interval of MHD simulations	3.63×10^{-6} $\times10^{-4}$ [s]

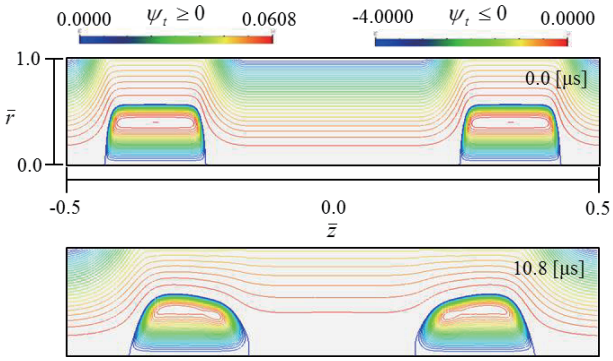

Fig. 2 The poloidal flux profile in the r–z plane. (Top) $t = 0$ [μs], (bottom) $t = 10.8$ [μs].

We solved the Grad–Shafranov equation in order to obtain an initial equilibrium state, in which the pressure follows a quadratic function of the magnetic flux and the initial toroidal magnetic field is assumed to be zero. We considered a case in which the initial plasma temperature is uniform; therefore, the mass density profile is similar to that of the plasma pressure. The equilibrium state of the single FRC plasma was solved for half of the calculation region so that the axial derivative of the flux becomes zero on the axial end and midplane $\bar{z} = 0.0$ (i.e., the axial position of the collision surface). Moreover, the obtained equilibrium flux profile is mirrored on the other half so as to fulfill the symmetry conditions. The device and plasma parameters are listed in Table 1. In the translation experiments, a sequential change of the external field caused an axial acceleration of the FRC plasma. With respect to the temporal change of the external field, the computational model described in [10] is used herein in the same manner. According to this model, the mirror field region of the upstream side gradually approaches the FRC plasma. Subsequently, the FRC plasma is accelerated towards the downstream direction. The time evolution of the poloidal flux in the acceleration phase is shown in Fig. 2. The to-

tal flux reads $\psi_t = \psi_e + \psi_p$, where ψ_e is the magnetic flux generated by the external coil current and ψ_p is that generated by the plasma current and modified by the wall condition, see [10] for more details. It must be remarked that we defined $\psi_t \geq 0$ inside the separatrix. In order to suppress unfavorable numerical noises generated in the radial boundary, we simulated the translation process by the simple resistive MHD model for 10.8 μs. Then, the Hall-MHD simulation starts right after 10.8 μs in order to study its influence on the collision and the merging process.

3. Simulation Results and Discussion

In this section, we present the results obtained from the Hall-MHD simulations. The temporal evolution of the 2D poloidal flux profile is shown in Fig. 3. The top figure shows the flux profile just before the head-on collision between two FRCs at 19.6 μs, after applying an external coil current in order to obtain an axial acceleration. Magnetic reconnection is found to occur at 25.0 μs and 30.1 μs and is followed by a resistive decay phase at 40.0 μs. Before the head-on collision, the flux profile is distorted from the equilibrium shape. We found that the separatrix surface swells in the front side of each FRC. The separatrix surfaces of these two FRCs contact each other at nearly the same radius as the field becomes null. Although the magnetic reconnection starts at the contacting point after 25.0 μs, the x-points on the geometric axis still separate at 25.0 μs and 30.1 μs. In the resistive decay phase, which takes places at around 40.0 μs, we found a doublet-type flux profile with two field-null points inside the separatrix. In this calculation, we did not observe any singlet structure with a single field-null point after the merging process. However, the field-reversed structure found by the internal magnetic probe array installed on the midplane of the C-2 experimental device [11] disagrees with our simulation results. For this reason, and since particle effects may contribute to the merging process, a new hybrid simulation model that treats plasma ions as super-particles will be developed in the near future.

Our previous resistive MHD model [10] does not take into account any toroidal magnetic field and was formulated under the assumptions of axial symmetry and non-flowing initial equilibrium. However, the inclusion of the Hall term results in the evolution of the toroidal magnetic field and flow. In Fig. 4, the time evolution of the toroidal magnetic field is shown by the color contour plot including the isopleth lines of the poloidal flux, with 30 lines drawn outside the separatrix. It was found that the toroidal field is generated mostly near the field-null points at 19.6 μs during the head-on collision, and its direction is opposite between two FRCs. At 25.0 μs and 30.1 μs, the toroidal field weakens around the field-null points, and its local maximum and minimum points move to the periphery of the separatrix. Consequently, the Hall term, as a two-fluid effect, influences the toroidal field generation; and the sign of this field is related to the direction of the axial motion of the plasma inside the separatrix. The temporal change of the pressure profile is also shown in Fig. 5 by the color contour plot, in which the pressure is normalized by $|\psi_w|^2/(2\mu_0 r_w^4)$. An increase of approximately 20% with respect to the equilibrium pressure is found near the impact face of these two FRCs. The position of the pressure peak moves from the front to rear region between 25.0 μs and

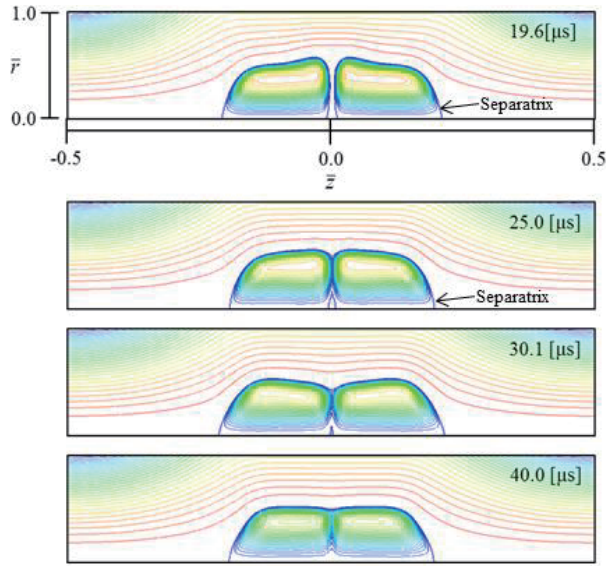

Fig. 3 Temporal change of the magnetic flux. (Top) t = 19.6 [μs], (the second) t = 25.0 [μs], (the third) t = 30.1 [μs], (bottom) t = 40.0 [μs].

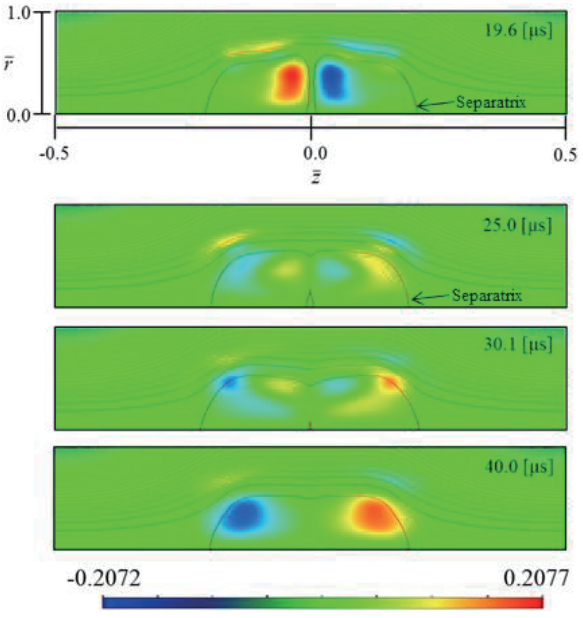

Fig. 4 Color contour plots of the toroidal magnetic field. (Top) t = 19.6 [μs], (middle) t = 25.0 [μs], (bottom) t = 30.1 [μs].

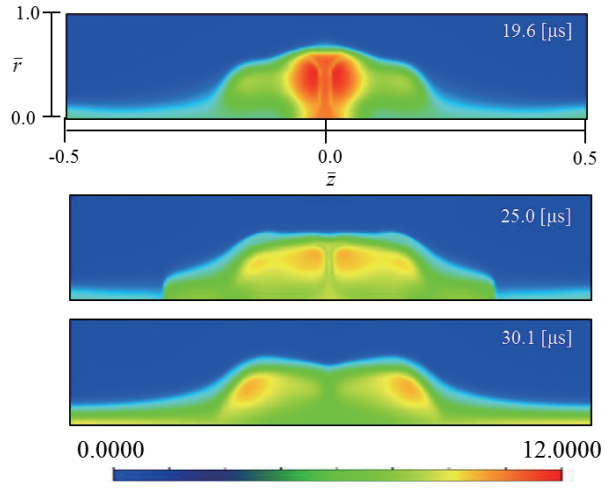

Fig. 5 Color contour plots of the pressure. (Top) t = 19.6 [μs], (middle) t = 25.0 [μs], (bottom) t = 30.1 [μs].

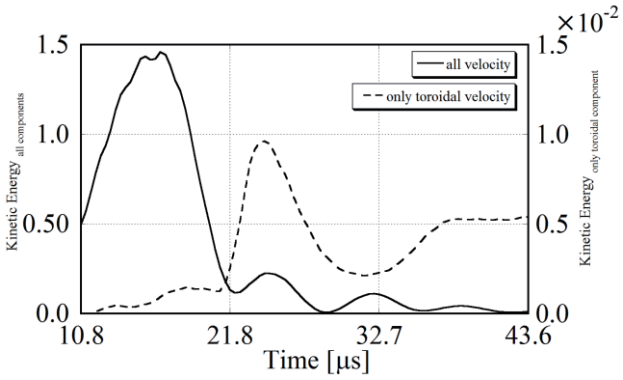

Fig. 6 Temporal evolution of the kinetic energy.

30.1 μs, which is thought to be an axial oscillating motion of the global structure caused by the collision.

Since our simulation model assumes a uniform temperature profile at the initial time, the Hall term in Eq. (4) is then zero by the vector identity, $\nabla \times \nabla\xi = \mathbf{0}$, where ξ is the arbitrary scalar function. Although the uniformity of the temperature gradually decreases, there is not much difference between the MHD results in [10] and the present Hall-MHD results.

In order to study the translation and collision process, we present the time evolution of the kinetic energy in Fig. 6 and the magnetic energy in Fig. 7 starting at 10.8 μs, when the Hall-MHD simulation starts. The volume averaged values can be calculated as follows:

$$\left\langle \frac{1}{2}\rho v^2 \right\rangle = \frac{\iint_V \frac{1}{2}\rho v^2 r\,\mathrm{d}r\,\mathrm{d}z}{\iint_V r\,\mathrm{d}r\,\mathrm{d}z},$$

$$\left\langle B^2/(2\mu_0) \right\rangle = \frac{\iint_V B^2/(2\mu_0)\, r\,\mathrm{d}r\,\mathrm{d}z}{\iint_V r\,\mathrm{d}r\,\mathrm{d}z}.$$

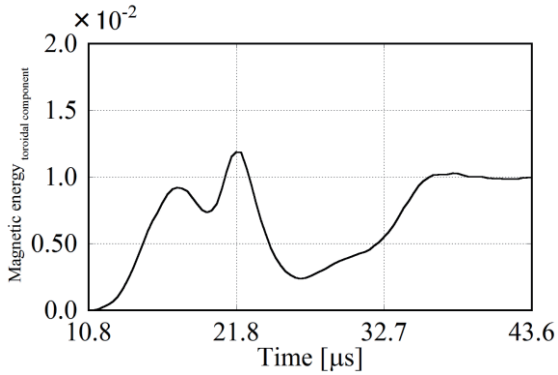

Fig. 7 Temporal evolution of the toroidal magnetic energy.

In this work, the volume integral is calculated inside the separatrix (i.e. the region with $\psi_t \geq 0$).

In Fig. 6, it can be seen that the axial acceleration vanishes at 16.7 μs and the kinetic energy rapidly decreases due to the deceleration caused by the interaction between FRCs. After the collision at 21.8 μs, the oscillation of the kinetic energy and its subsequent relaxation process is evidenced. The period of the axial oscillatory motion is about 7 μs. The dashed line depicted in Fig. 6 indicates the kinetic energy by the toroidal component of the flow velocity. It is found that the kinetic energy from the toroidal flow increases rapidly after the collision and reaches its peak at 24.3 μs. We also noticed that the toroidal flow energy yields a steady value as the relaxation process starts. It is thought that the plasma relaxes to a state of quasi-equilibrium with a weak toroidal flow.

The time evolution of the magnetic energy, considering only the toroidal component, is shown in Fig. 7. From this figure, it can be found that the toroidal field gradually increases during the translation phase. Moreover, the field reaches the peak at the axial collision and is generated near the colliding surface, as shown on the top of Fig. 4. Although the toroidal field weakens in 19.6 $\leq t$ [μs] $\leq$ 25.0, it increases again as the relaxation process proceeds ($t \geq$ 25.0 μs). Finally, the stable toroidal field remains in the axial end region of the merged FRC plasma, as shown on the bottom of Fig. 4.

To find a quantitative Hall-MHD effect, we show the difference in the current density profile on the midplane between the resistive and the Hall-MHD simulation results, as shown in Fig. 8. When the vertical axis is positive, the current density from the Hall-MHD simulation is larger than that from the resistive MHD model. Negative values in the vertical axis imply that the magnitude of the opposite current density generated in the reconnection region becomes larger than the reference current from the resistive MHD model. The difference is slight for the whole radial range before the collision ($t \leq$ 19.6 μs), whereas a considerable difference is found after the collision. Due to the nature of our resistivity model in Fig. 1, a larger resistivity is used for the reconnection region $\bar{r} \leq 0.50$ and

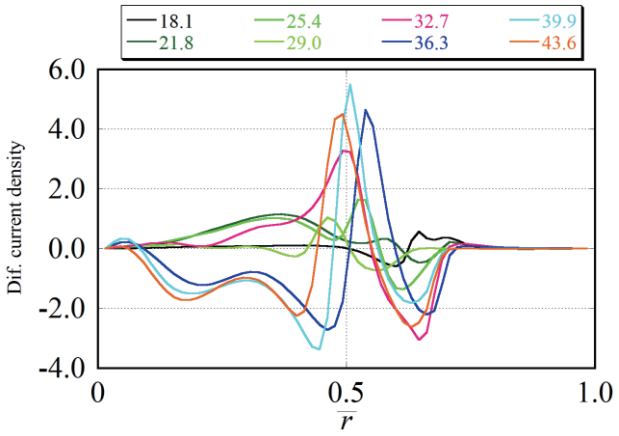

Fig. 8 Difference between the current density profiles on the midplane $\bar{z} = 0.0$ obtained from the Hall and resistive MHD models.

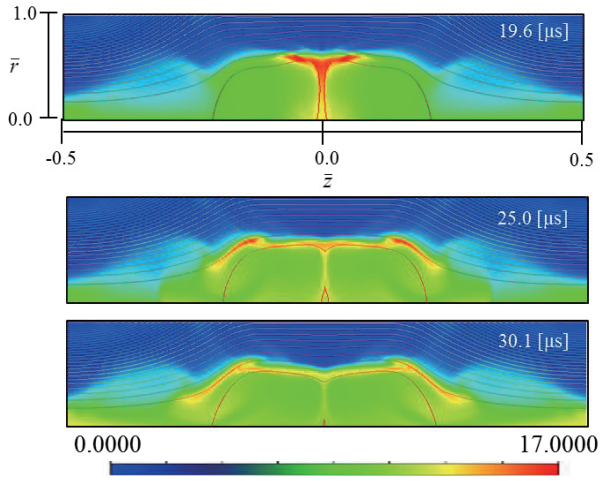

Fig. 9 Color contour of the normalized temperature. (Top) t = 19.6, (middle) t = 25.0, (bottom) t = 30.1 [μs].

phase, if the difference in Fig. 8 is negative. Therefore, the magnetic diffusion process for the Hall-MHD model is faster than that for the resistive MHD model when Eq. (5) is used for both cases.

4. Summary and Future Works

In the present paper, we have reported the results from Hall-MHD simulations for FRC translation by a sequential external field control [10], axial collision between two accelerated FRCs, and a merging process. It has been found that a weak toroidal field is mainly generated during the translation phase. When the plasma resistivity is assumed to be a function of the current density and becomes larger as the current in the reconnection region increases, the Hall-MHD model tends to lead to a faster reconnection.

In the present calculation, however, we did not observe plasma heating in the core region. The 2D plasma temperature profiles at three separate times are shown in Fig. 9. From this figure, it is found that the plasma temperature is elevated only in the edge region. Conversely, there is no considerable increase in the core region. The heated region moves along the open-field region, and thus no thermal conduction toward the plasma core occurs. Contrary to our simulation results, a significant heating process is obtained from the Lamy Ridge code as seen in [3]. We consider that a significantly large thermal conductivity, as a cross-field transport mechanism, is needed for core heating. Future studies will be devoted to the analysis of the presence of such a large conductivity.

Acknowledgements

This work is performed with the support and under the auspices of the NIFS Collaborative Research Program (NIFS14KNWP004, NIFS15KNTT033, and NIFS15KNST087). The authors would like to thank Enago (www.enago.jp) for the English language review.

[1] M. Tuszewski, Nucl. Fusion **28**(11), 2033 (1988).
[2] M.W. Binderbauer, H.Y. Guo, M. Tuszewski *et al.*, Phys. Rev. Lett. **105**(4), 045003 (2010).
[3] H.Y. Guo, M.W. Binderbauer, D. Barnes, S. Putvinski, N. Rostoker *et al.*, Phys. Plasmas **18**, 056110 (2011).
[4] G.A. Wurden, K.F. Schoenberg, R.E. Siemon, M. Tuszewski, F.J. Wysocki and R.D. Milroy, J. Plasma Fusion Res. SERIES **2**, 238 (1999).
[5] R.D. Milroy, A.I.D. Macnab, C.C. Kim and C.R. Sovinec, J. Fusion Energy **27**, 73 (2008).
[6] M. Yamada, R. Kulsrud and H. Ji, Rev. Mod. Phys. **82**(1), 603 (2010).
[7] Y. Ono, M. Inomoto, Y. Ueda, T. Matsuyama and T. Okazaki, Nucl. Fusion **39**, No.11Y, 2001 (1999).
[8] E.N. Parker, J. Geophysical Research **62**(4), 509 (1957).
[9] R.M. Kulsrud, Earth Planets Space **53**, 417 (2001).
[10] K. Matsuzaki *et al.*, IEEJ Trans. Fundam. Mater. **135**, 296 (2015).
[11] H. Gota *et al.*, Rev. Sci. Instrum. **83**, 10D706 (2012).